Shock, Publish Ahead of Print
DOI: 10.1097/SHK.0000000000001494

REGULATORY ROLES OF HUMAN SURFACTANT PROTEIN B VARIANTS ON GENETIC SUSCEPTIBILITY TO *Pseudomonas aeruginosa* PNEUMONIA-INDUCED SEPSIS

Fengyong Yang[*,†], Jing Zhang[*], Yi Yang[#], Feng Ruan[*], Xinghua Chen[*], Junping Guo[*], Osama Abdel-Razek[*], Yi Y. Zuo[#], Guirong Wang[*,¶]

[*]Department of Surgery, [¶] Department of Microbiology and Immunology, SUNY Upstate Medical University, Syracuse, NY, 13210, USA

[†]ICU, Jinan People's Hospital, Jinan 271199, Shandong Province, P. R. China

[#]Department of Mechanical Engineering, University of Hawaii at Manoa, Honolulu, HI 96822, USA

Corresponding author:

Guirong Wang, PhD (Dr. rer. Nat.), Department of Surgery, UH Room 8715
SUNY Upstate Medical University
750 E Adams St, Syracuse, NY, 13210, USA ; Phone: 315-464-6283 ; Fax: 315-464-6236
E-mail: wangg@upstate.edu

This study is supported by NIH R01HL136706 and in part by the NSF research award (1722630) (to GW).

This study was selected as one of the New Investigator Nominees at the 42nd Annual Conference on Shock, held in Coronado, California, June 8-11, 2019.

The authors have no relevant conflicts of interest.

Abstract

Surfactant protein B (SP-B) is essential for life and plays critical roles in host defense and lowering alveolar surface tension. A single nucleotide polymorphism (SNP rs1130866) of human SP-B (hSP-B) alters the N-linked glycosylation, thus presumably affecting SP-B function. This study has investigated the regulatory roles of hSP-B genetic variants on lung injury in pneumonia-induced sepsis. **Methods**: Wild-type (WT) FVB/NJ and humanized transgenic SP-B-T and SP-B-C mice (expressing either hSP-B C or T allele without mouse SP-B gene) were infected intratracheally with 50μl (4×10^4 CFUs/mouse) *Pseudomonas aeruginosa* Xen5 or saline, then sacrificed 24 hrs or 48 hrs after infection. Bacterial dynamic growths were monitored from 0 to 48 hrs post-infection by *in vivo* imaging. Histopathological, cellular and molecular changes of lung tissues and bronchoalveolar lavage fluid (BALF) were analyzed. Surface tension of surfactants was determined with constrained drop surfactometry. **Results**: SP-B-C mice showed higher bioluminescence and CFUs, increased inflammation and mortality, the higher score of lung injury, reduced numbers of lamellar bodies in type II cells compared to SP-B-T or WT ($P<0.05$). Minimum surface tension increased dramatically in infected mice ($P < 0.01$) with the order of SP-B-C>SP-B-T>WT. Levels of multiple cytokines in the lung of infected SP-B-C were higher than those of SP-B-T and WT ($P < 0.01$). Furthermore, compared to SP-B-T or WT, SP-B-C exhibited lower SP-B, higher NF-κB and NLRP3 inflammasome activation, and higher activated caspase-3. **Conclusion:** hSP-B variants differentially regulate susceptibility through modulating the surface activity of surfactant, cell death and inflammatory signaling in sepsis.

Keywords: Acute Lung Injury; ARDS; Human SP-B Genetic Variants; NF-κB/NLRP3 signaling, *Pseudomonas aeruginosa*; Surfactant Activity

Introduction

Surfactant protein B (SP-B), a key component of surfactant, is essential for normal lung respiratory physiology. It plays critical roles in lowering surface tension to prevent alveoli from collapse and host defense against bacterial infection (1, 2). Human SP-B gene (*sftpb*) contains several genetic variations, including a critical single nucleotide polymorphism (SNP rs1130866), which has a nucleotide T to C transition. The nucleotide transition of the SNP alters the N-linked glycosylation status of the Asn^{129} site in pro-SP-B protein, i.e., the SP-B C allele with the additional N-linked glycosylation site but not in the T allele (3, 4). This altered glycosylation may have an implication on SP-B protein processing and function under disease or stress conditions, although both C and T alleles are common SP-B genetic variation in the general population (5, 6). Genotyping-association studies of patients demonstrated that patients with C allele are more susceptible than those with T allele to pneumonia and pneumonia-induced acute respiratory distress syndrome (ARDS) (7-9). However, the mechanisms underlying differential susceptibility of human SP-B genetic variants to pneumonia-induced acute lung injury (ALI) and ARDS are unclear yet (10, 11).

SP-B gene belongs to a member of Saposin-like protein (SAPLIN) family, which is involved in multiple functions such as lipid interaction and antimicrobial activity (2, 12). The SP-B precursor contains three SAPLIN domains: the first two domains produced two mature proteins i.e., $SP\text{-}B^{N}$ and $SP\text{-}B^{M}$, which are involved in host defense and surface tension, respectively (2). While the function of the other SAPLIIN domain, which locates in C-terminal ($SP\text{-}B^{C}$) region, is not known yet (2). SP-B expression is restricted to the alveolar type II cells and Club cells in the respiratory epithelium. The processing of pro-SP-B precursor to mature SP-B in type II cells in the lung requires proteolytic cleavages and a series of post-translational modifications, including glycosylation. The mature SP-B protein should be transported into the lamellar body, which consists of surfactant-specific phospholipid and other proteins (13, 14).

Humanized mouse models have proven to be powerful tools in the study of many human biological processes and excellent models for pre-clinical testing. Humanized transgenic (hTG) mouse model has helped overcome the limitation in the study of human biology *in vivo*. The physiological and pathological functions of human gene/variants (alleles) can be investigated in the complex biological or pathological processes using hTG mouse method (15, 16). In the past

several years, we have generated and characterized hTG SP-B mice, i.e., SP-B-C and SP-B-T mice, which expressed either human SP-B C or T allele without mouse SP-B gene (17, 18). These hTG mice have provided us an excellent tool to elucidate the cellular and molecular mechanisms of the regulatory roles of human SP-B genetic variants on the differential susceptibility in response to bacterial-induced ALI/ARDS.

Pseudomonas aeruginosa, a gram-negative bacteria, is a clinically relevant pathogen, especially in the patients with ventilator-associated infection and in cystic fibrosis. Previous studies demonstrated that the FVB/N strain of mice is sensitive to this pathogen, although one common laboratory strain PA01 has moderate toxicity to mice (19, 20). In order to establish a severe septic mouse model and to monitor *in vivo* bacterial growth, we have employed one *P. aeruginosa* strain Xen5 with high toxicity and expressing bioluminescence in this study. Using the pneumonia-induced ARDS model, we tested our hypothesis that SP-B genetic variants have differentially regulatory roles in the pathogenesis of ALI/ARDS. We examined dynamic bacterial growth *in vivo*, cellular and molecular changes, as well as surfactant dysfunction in the lung of the three types of mice after intratracheally bacterial infection by various cellular and molecular methodology. The findings from the present study demonstrated that human SP-B genetic variants differentially regulate susceptibility to pneumonia-induced ALI/ARDS through influencing bacterial growth and surfactant activation, modulating host cell death, inflammation, and inflammatory NF-κB signaling pathway.

Materials and Methods

Mice

We employed hTG SP-B-C and SP-B-T (FVB/N strain background) and wild-type FVB/N in this study. hTG SP-B-C and SP-B-T, carrying either human SP-B C or T allele without mouse SP-B gene were generated in our laboratory; the genotypes and human SP-B expression were confirmed by PCR and Western blot as described as published previously (17). Original WT FVB/N mice were purchased from the Jackson Laboratory (Bar Harbor, ME) and were bred for experimental use. All the animals were maintained under the pathogen-free condition in the animal core facility at SUNY Upstate Medical University, with a standard 12 h/12 h light/dark time cycle, the stable-controlled temperature at 24℃, and regular mouse chow and water *ad*

libitum. Both male and female mice of each type (8-12 weeks old, about 25 g bw) were used for the experiments. In this study, each genetic variant (SP-B-C, SP-B-T and WT) of mice was divided into two groups: the pneumonia group (infected with *P. aeruginosa* Xen5 strain) and the control group (the sham group with same surgery and the same volume of the sterile vehicle given). All the related animal protocols were strictly adhered to according to with National Institutes of Health and ARRIVE guidelines and approved by the Institutional Animal Care and Use Committee of SUNY Upstate Medical University (IACUC#380).

P. aeruginosa-induced mouse sepsis

The pneumonia-induced sepsis model was established intratracheally by injecting 50µl of bioluminescent *P. aeruginosa* Xen5 solution (about 4×10^4 CFU/mouse) based on several pilot experiments. The optimal dose of *P. aeruginosa Xen5* used in this study are appropriate for *in vivo* imaging analysis and induced ARDS and about 50% of survival rate 48h post-infection. In brief, a single colony of *P. aeruginosa Xen5* was cultured in 5 ml of LB liquid medium at 37ºC, 250 RPM incubator overnight. Bacterial pellets were obtained from a subculture of the bacteria. Then pellets were resuspended with cold saline buffer and adjusted to OD_{600} value to 0.6. The bacterial solution was diluted 500 times for animal infection. Each mouse was injected 50µl of the bacterial solution for the infection group or the same size of sterile saline with the same surgery for the control group. The procedures of anesthesia, surgery and intratracheal inoculation of bacteria were performed as described previously (18, 21).

In vivo imaging analysis

Bacterial dynamic changes were detected by monitoring the bioluminescence signaling at 0, 12, 24, 36 and 48 hrs post-infection by *in vivo* imaging system (Caliper Life Science, Hopkinton, MA) as described previously (18, 22). All the measurement was performed following the same imaging setting mode: i.e., Exposure time, 3 min; Binning, large; F/stop, 1.

Mouse specimen collection

Mice were anesthetized with ketamine/xylazine cocktail (90 mg/kg ketamine, 10 mg/kg xylazine) by intraperitoneal injection and be sacrificed by exsanguination. Blood was collected from the inferior vena cava using a 1-ml syringe. Lung tissue and bronchoalveolar lavage fluid

(BALF) were harvested as described previously (18, 23). In order to obtain BALF, each lung was lavaged with 0.5 ml of cold saline and repeated three times. About 1.2ml of BALF per mouse was obtained as previously described (18, 22, 23).

Histopathological analysis

Lung tissues were fixed for 24 hrs and then were embedded into paraffin. Sections (about 5μm) of lung tissues were prepared and stained with hematoxylin and eosin (H&E). Lung injury score was blindly determined by two experienced investigators (22, 23).

Ultrastructural analysis by transmission electron microscopy

Analysis of the ultrastructural properties of lung cells was performed as described previously (23). In brief, lung tissues were fixed by 2.5% glutaraldehyde and 2% paraformaldehyde in 0.1 M phosphate buffer (pH 7.4) and further fixed in 1% osmium tetroxide in 0.1 M phosphate buffer (pH 7.4) for 1 hour. Samples dehydrated and embedded in LX-112 (Ladd Research Industries, Vermont, VA). Thin sections (70nm) were cut and stained with uranyl acetate and lead citrate. Samples were viewed in a JEOL JEM1400 TEM (JEOL USA Inc., Peabody, MA, USA). Each sample was examined at various magnifications from 6,000X to 35,000X.

Bacterial CFUs

Bronchoalveolar lavage fluid (BALF) of each mouse was obtained as described above. To determine bacterial numbers in the BALF, fresh BALF (100 μl) from each mouse was diluted at 1000 times, and then 100 μl of diluted BALF was plated on LB-Agar plates. Experiments were performed by triplicates for each mouse, and the CFUs for each mouse was calculated by an average of CFU counts from three plates. Plate cultures were incubated overnight at 37ºC, and colony counts were then determined. Total CFUs were calculated and expressed CFUs per lung (21).

Inflammatory cell analysis in BALF

Quantification of inflammatory cells from BALFs were performed as described previously (21-23). In brief, BALF sample was prepared from individual animals (n=8 mice per group). About 10 μl of each fresh BALF was used for total cell counting with a hemocytometer. The remaining

BALF samples were centrifuged for 10 min at 250xg at 4°C. The cell pellet was re-suspended with 1 ml of cold sterile saline. The cells in 200 µl re-suspended cell solutions were mounted on a slide by cytospin centrifugation at 1000 rpm for 3 min. Cells were stained using the Protocol HEMA-3 cell staining kit (Fisher, Pittsburg, PA). Macrophages/monocytes and polymorphonuclear neutrophils (PMNs) on the slides were identified and quantified by Nikon 2000 research light microscope (× 200 magnification).

Analysis of the surface activity of pulmonary surfactants

The cell-free supernatant from the first time centrifugation was followed by a second time high-speed centrifugation for 15 min at 40,000x*g* at 4°C. The large aggregates (LAs) were re-suspended in 0.1 mL buffer (140 mM NaCl, 2.5 mM $CaCl_2$, and 10 mM HEPES and at pH 6.9), and they were adjusted to a phospholipid concentration of 1 mg/mL (17, 24). The surface activity of the LAs was determined as previously described, using constrained drop surfactometry (CDS) (25, 26). In CDS, the adsorbed pulmonary surfactant film is accommodated at the air-water surface of a sessile droplet (~4 mm in diameter, ~16 µL in volume, and ~0.25 cm^2 in surface area), which is "constrained" on a carefully machined pedestal. The pedestal has a knife-sharp edge that prevents film leakage and keeps the droplet integrity even at near-zero surface tensions. The surfactant film can be compressed and expanded periodically via regulating the surface area of the droplet by controlling liquid flow into and out of the droplet with a motorized syringe. The droplet is small enough to be enclosed in an environmental control chamber that permits simulations of physiologically-relevant intra-alveolar conditions, *i.e.*, the core body temperature of 37 ºC and relative humidity close to 100%. Specifically, a 16 µL surfactant droplet was dispensed onto the CDS pedestal via a pipette. The surface tension decrease during film adsorption was recorded until an equilibrium value of around 23 mN/m was reached. The adsorbed surfactant film was then compressed and expanded at a rate of three seconds per cycle to simulate normal tidal breathing. The surface tension and surface area of the surfactant film were determined simultaneously using closed-loop axisymmetric drop shape analysis (CL-ADSA) (26). The minimum surface tension (γ_{min}) during dynamic cycling was reported as an indication of surface activity.

Cytokine analysis by ELISA

Mouse lungs were harvested 24 hrs post-infection, then lung tissues were homogenated in cold saline and centrifuged at 12,000xg at 4ºC for 20 min by Eppendorf centrifuge. The supernatant was used for ELISA assay. The ELISA analysis was performed with a Muti-Analyte ELISArray Kit (QIAGEN, Germantown, MD), which can analyze a panel of 12 pro-inflammatory cytokines simultaneously using a conventional ELISA protocol. The cytokines analyzed in this study include IL-1α, IL-1β, IL-2, IL-4, IL-6, IL-10, IL-12, IL-17A, IFN-γ, TNFα, G-CSF, and GM-CSF.

TUNEL assay

TUNEL assay of the sections of lung tissues was performed with the TUNEL kit (Roche, Indianapolis, IN) following the protocol, as described previously (22). Apoptotic cells were quantified by counting TUNEL-positive cells in 20 random fields of light microscopy at 200X magnification.

Immunofluorescence (IF) analysis

To detect the protein SP-B, NLRP3 and pNF-κB p65 expression in the cells of lung tissue, immunofluorescence staining was performed with the paraffin-embedded lung sections on slides and anti-SP-B antibody (1:100, Hycult biotech, Plymouth Meeting, PA), NLRP3 antibody(1:50, ThermoFisher Scientific, Rockford, IL) , p-NF-κB p65 (1:300, CST, Boston, MA) as described previously (22).

Western blotting analysis

The Western blotting analysis was performed following our previous description (23). In brief, protein samples were prepared from lung tissues with RIPA buffer containing a cocktail of protease and phosphatase inhibitors. Total protein concentrations of samples were determined by the micro-BCA method. Protein samples (50μg of protein per lane) were separated by 12% SDS-polyacrylamide gel electrophoresis under reducing (for phosphorated NF-κB p65, i.e., pNF-κB p65, Caspase-3) or non-reducing (for SP-B) condition. The PVDF membrane (Bio-Rad, Hercules, CA) was blocked with 5% non-fat milk of Tris-buffered saline, then followed by primary antibody, Caspase-3 (1:1000, CST, Boston, MA), pNF-κB p65 (1:1000, CST, Boston,

MA), anti-SP-B antibody (1:2000, Hycult biotech, Plymouth Meeting, PA), the secondary HRP-conjugated antibody (Bio-Rad, Hercules, CA). After finishing incubation and washing, the signal of protein was detected with Pierce ECL Western Blotting detection reagent (Thermo Scientific, Rockford, IL), then exposed to X-film in a darkroom. For the internal control, the blot was stripped and reprobed with β-actin antibody (1:2000, Abcam, Cambridge, MA). The band on the film was quantified by scanning the film with the Quantity One software (Bio-Rad, Hercules, CA).

Statistical analysis

Data were expressed as means ± SEM in this study. All statistics were performed with SigmaStat Software (version 3.5). The comparisons among the three groups of mice were analyzed by one-way ANOVA, and then the pairwise comparison was performed using Student's t-test. The survival analysis of animals was performed with Kaplan-Meyer survival curves and examined statistically by the Log-rank test. There are significant differences when $P < 0.05$.

Results

Bacterial dynamic changes in vivo in the lung of infected mice

To examine dynamic bacterial growth *in vivo P. aeruginosa* Xen5 expressing with bioluminescence was used for lung infection of three types of mice, i.e., hTG SP-B-C, SP-B-T and WT mice. Total bioluminescence flux detected by *the in vivo* imaging system represents the bacterial burden in the lung of infected mice. The total flux of three types of infected mice was monitored at 0, 12, 24, 36, and 48 hrs post-infection of three types of infected mice. The representative images of several time points of three types of infected mice were shown in Figure 1A. Bacterial burden increased dramatically starting 12 hrs post-infection in all three types of mice; the level of bacterial burden was the highest in SP-B-C mice compared to SP-B-T and WT mice at 12, 24, 36 and 48 hrs post-infection ($P < 0.01$) (Fig. 1B). Furthermore, the CFUs of bacteria were determined in the BALF of mice at 24 hrs post-infection, the results showed similar pattern observed in the *in vivo* imaging method; the CFUs in the lung of SP-B-C was the highest among three types of mice (i.e., SP-B>SP-B-T>WT) ($P < 0.01$); as expected, no bacteria were detected in controls (Fig. 1C). In addition, we also analyzed the survival rate in this study;

SP-B-C mice had higher mortality rate compare to SP-B-T ($P < 0.05$) and WT mice ($P < 0.01$), respectively; no mortality of sham mice was found (Fig. 1D), suggesting differential susceptibility of three types of mice in response to pneumonia-induced sepsis.

Inflammatory cells in BALF

In order to assess the inflammatory cell filtration into lung alveoli after infection, total cell counts were assessed in the BALF of infected mice and controls. Inflammatory cells (macrophages and neutrophils) were quantified in the sections prepared by cytospin centrifugation. As expected, only macrophages were observed in the BALF from controls; but more than 90% of inflammatory cells were neutrophils in the BALF from infected mice (Fig. 2A). Total cell counts in BALF increased significantly after infection compared to controls ($P < 0.01$), and the SP-B-C mice had the most significant number of total cell counts among three types of infected mice, i.e., SP-B-C>SP-B-T>WT ($P < 0.01$) (Fig. 2B).

Histopathological analysis of lung injury

Lung histopathologic changes were assessed in the H&E staining sections of infected mice and controls, lung injury scores of three types of mice were calculated as described previously (18, 22, 23). We have observed remarkable lung injury in infected mice but not in controls, the injurious lung showed large amounts of inflammatory cells in alveolar spaces and interstitials, proteinaceous debris accumulation and the thicker alveolar wall (Fig. 2C). The injury score of each type of infected mice was significantly higher than that of each control group ($P < 0.01$); and infected SP-B-C mice had higher injury score compared to infected SP-B-T ($P < 0.05$) and WT mice ($P < 0.01$) (Fig. 2D).

Ultrastructural analysis of lung injury

To examine the ultrastructural changes of cells in the lung after bacterial infection, the ultrastructural properties of the lung cells were assessed by transmission electron microscopy at various magnifications from 6,000X to 35,000X. There were many normal lamellar bodies and healthy mitochondria in the alveolar epithelial type II cells in all controls, suggesting human SP-B genetic variants are functional in mice (Control Panel of Fig. 3A). However, it was observed increased autophagosomes, and damaged lamellar bodies and abnormal mitochondria as well as decreased microvilli in type II cells in infected mice (Pneu Panel of Fig. 3A). The quantitative analysis indicated that there is a significantly reduced number of lamellar bodies in type II cells of infected mice compared to the controls ($P < 0.01$). The number of lamellar bodies of infected SP-C was less than that of infected SP-B-T and WT mice ($P < 0.01$) (Fig. 3B).

Apoptosis in the lung of infected mice

We examined apoptosis in the lung of three types of infected mice using TUNEL assay and Western blotting analysis. As shown in Figure 4, remarkable apoptotic cells showed in red color were detected in the images of TUNEL assay in the lung of infected mice but not in the lung of controls (Fig. 4A). The data from Western blotting analysis with anti-caspase-3 showed an increased level of activated caspase-3 (a band with 17 kDa) in all infected mice (Fig. 4B). The quantitative analyses indicated that there is a significant increase of apoptotic cells in the lung of infected mice compared to the controls ($P < 0.01$), and there are differences among three types of infected mice, i.e., SP-B-C>SP-B-T>WT ($P < 0.01$) (Fig. 4C). The level of activated caspase-3 in infected SP-B-C was higher than that of SP-B-T and WT mice ($P < 0.01$) (Fig. 4D).

Decreased SP-B expression in the lung of infected mice

SP-B protein is essential for life through lowering surface tension and host defense in the alveolar space of the lung. We examined the SP-B expression and its level in the lung by IF and Western blotting analyses. As shown in Figure 5, many IF positive cells were detected in the lung tissues of hTG SP-B-C, SP-B-T, WT mice but there were decreased IF positive cells in the

lung of infected mice (Fig. 5A); the results from Western blotting with anti-SP-B antibody further confirmed decreased SP-B level in all three types of infected mice compared to the controls (Fig. 5B). The quantitative analyses of IF images indicated a significant decrease of IF positive cell number per HPF in the infected mice compared to the controls ($P < 0.01$) and there were differences among three types of infected mice, i.e., SP-B-C<SP-B-T<WT ($P < 0.01$) (Fig. 5C). Furthermore, the level of SP-B protein from quantitative analysis of the Western blot indicated a significant decrease in the infected mice compared to the controls ($P < 0.01$) and there were differences among three types of infected mice ($P < 0.05$) but not in controls (Fig. 5D).

Compromised surface activity of pulmonary surfactants of infected mice

SP-B is a critical component of pulmonary surfactant that helps lower alveolar surface tension, thus preventing lung collapse and closure of small airways in the distal lung. We examined the surface activity of large aggregates (LAs) extracted from the BALF of infected mice and the controls using CDS (see Methods). Panel A of Figure 6 showed the dynamic cycling results in which the surface tension changes as a function of rapidly decreased and increased surface area that simulates tidal breathing. Panel B of Figure 6 showed the statistical analysis of the minimum surface tension (γ_{min}) obtained at the end of film compression during the dynamic cycling process. It was found that the γ_{min} of the infected mice increased significantly compared to the control mice. Besides, we found that the γ_{min} of the three infection groups ranks in the order of SP-B-C>SP-B-T>WT ($P < 0.05$), which suggests differential regulation of hSP-B genetic variants to the alveolar surface tension under infectious conditions.

Multiple cytokine analysis in the lung of infected mice

Inflammatory cytokine expression is a remarkable character in pneumonia and pneumonia-induced sepsis. We examined a total of 12 cytokines, which are in response to bacteria-induced lung inflammation and injury, with lung homogenates of infected (24h post-treatment) mice and controls by a Muti-Analyte ELISArray Kit. Out of 12 cytokines, nine, i.e., TNF-α, IL-6, IL-1α,

IL-1ß, G-CSF, GM-CSF, IFN-γ, IL-4 and IL-12 increased significantly in infected mice when compared to the controls ($P < 0.01$) (Fig. 7). Furthermore, the levels of TNF-α, IL-6, IL-1α, IL-1ß of infected SP-B-C mice were higher than those of infected SP-B-T and WT mice ($P < 0.05$ or $P<0.01$) (Fig. 7), indicating differential regulation of proinflammatory cytokines between human SP-B genetic variants. By contrast, there was no difference of G-CSF, GM-CSF, IFN-γ, IL-4 and IL-12 among three types of infected mice. We also found no significant changes in the levels of IL-2, IL-10, IL-17A between infected mice and the controls (Data not shown).

Inflammatory NF-κB signaling activation in the lung of infected mice

Previous studies have demonstrated that the activation of the NF-κB signaling pathway plays a critical role in the host defense and inflammatory response to the bacterial infection and sepsis (18, 27). We examined the NF-κB activation by IF and phosphorated NF-κB p65 (pNF-κB p65), the critical component of the NF-κB signaling pathway by Western blotting analysis. As shown in Figure 8, both IF and Western blotting analyses showed increased NF-κB activation in infected mice compared to the controls. Furthermore, different levels of NF-κB activation were observed among three types of infected mice, indicating that infected SP-B-C mice showed higher level compared to infected SP-B-T ($P < 0.05$) and infected WT mice ($P < 0.01$), respectively.

Increased NLRP3 inflammasome activation in the lung of infected mice

We examined the NLRP3 inflammasome activation in the lung of infected mice and the controls by IF. As shown in Figure 9, increased NLRP3 IF positive cells were detected in the infected mice compared to the controls, and different levels of NLRP3 inflammasome activation were observed among three types of infected mice, i.e., infected SP-B-C mice had more positive cells compared to infected SP-B-T and infected WT mice ($P < 0.01$). The results of NLRP3 inflammasome activation analysis were consistent with the observation of NF-κB activation in this study.

Discussion

Pneumonia-induced sepsis is a major cause of ARDS and multiple organ dysfunction, which have very high associated mortality (40-60%). Some individuals are more susceptible to bacterial pneumonia-induced sepsis compared to others, but the underlying mechanisms are unclear. Human genomic variation, including human SP-B genetic variants, should contribute to the susceptibility and disease severity of ARDS and sepsis because SP-B protein is essential for maintaining formal surfactant activity and host defense in the lung. Patients-based genotyping studies have demonstrated the association of hSP-B polymorphisms with pneumonia-induced ALI/ARDS, and the decreased level of SP-B protein was used as an essential biomarker of ARDS progression (10, 11). In the present study, we investigated the regulatory roles of hSP-B genetic variants on the lung injury and surface activity of pulmonary surfactant in the *P. aeruginosa*-induced mouse septic model. We found differentially regulatory effects of hTG SP-B C and T alleles in response to bacteremia through influencing *in vivo* bacterial growth, regulating inflammatory cells and molecular processes, as well as surfactant activation in the lung.

SP-B, an essential protein of pulmonary surfactant, causes lethal respiratory failure when an acute reduction by about 60% of normal levels occurs in animals (28) or ARDS patients (10). The SP-B precursor can produce two proteins, i.e., $SP\text{-}B^{M}$ and $SP\text{-}B^{N}$, which are involved in lowering surface tension and innate host defense, respectively (2). Several hSP-B polymorphisms and mutations have been identified, including the SNP (rs1130866), one of the most important SNPs (9, 29). This SNP is associated with several pulmonary diseases, including pneumonia and pneumonia-induced ARDS (7-9), neonatal respiratory distress syndrome (RDS) (30). Our findings from this study demonstrated the C allele of hSP-B exhibited decreased host defense and increased compromised surface activity of pulmonary surfactant in the infected mice compared to the T allele. These *in vivo* results from our septic hTG mouse model are consistent with the observations of patients-based genotyping analysis (6), indicating the regulatory roles of the hSP-B genetic variants due to the SNP rs1130866 in the pathogenesis of septic ALI/ARDS.

hTG mice has provided an ideal tool to explore biological function and variation of human gene/allele in the pathophysiological processes, which is able to overcome the limitation of human beings, for example, to test *in vivo* capacity and the mechanisms of human gene/allele in response to various infectious conditions (15, 31). In this study we found no difference of the

surface activity of pulmonary surfactants (minimum surface tension) and lung structural properties among three types of mice, i.e., SP-B-C, SP-B-T and WT mice in normal conditions (control groups), indicating that human SP-B variants function well in the transgenic mice. Furthermore, higher bacterial load, increased inflammatory cells and proinflammatory cytokine expression were observed in the lungs of infected SP-B-C mice when compared to infected SP-B-T and WT mice in the present study, suggesting the decreased innate immune ability of SP-B C allele in comparison with the T allele, as well as WT mice.

The previous studies demonstrated that the process of producing mature SP-B protein is involved in complex SP-B precursor processing and differentially complicated posttranslational modification (32). Other surfactant lipids and proteins, including mature SP-B, are packaged into lamellar bodies from which surfactants are secreted into the air space by exocytosis (3). The SNP (rs1130866) can result in the alteration of N-linked glycosylation of SP-B, thus may influence the level of mature SP-B by affecting the transfer of SP-B to lamellar bodies (32) and the efficiency of pro-SP-B cleavage under infectious or stress conditions (30). Lung ultrastructural analysis by electron microscopy revealed abnormal type II cells and many damaged lamellar bodies in the infected mice. However, it is necessary to investigate detailed molecular mechanisms further how the N-linked glycosylation in the C allele influences SP-B precursor processing and trafficking in the type II cells under infectious conditions.

SP-B plays a role in the host defense and surfactant physiology (33). The protein product (SP-B^N) produced from SP-B precursor recognized as an antimicrobial peptide, directly killed bacteria and indirectly promoted uptake of bacteria by macrophages. *In vivo*, the ability of bacterial killing was enhanced in over-expressing SP-B^N mice (34). *In vitro*, the growth of bacteria *Pseudomonas aeruginosa Xen5* was significantly inhibited when co-incubated with mice BALF while the effect reversed when SP-B^N IgG was added (2). The results from this study demonstrated that *P. aeruginosa* infection could cause cell death and induce proinflammatory cytokine expression by NF-κB-dependent transcriptional upregulation with increased NLRP3 and Caspase-3 activation. The data about NF-κB signaling activation and a panel of inflammatory cytokine expression in response to *P. aeruginosa* infection further revealed differential regulation of SP-B genetic variants on the lung injury. NF-κB is usually composed of the p50/p65 heterodimers and its effector form, phosphorylated NF-κB-p65, dissociates from

NF-κB complex, and then translocates into the nucleus upon stimulation. The protein of 17-kDa Caspase-3 is the active form of Caspase-3, recognized as an indicator of apoptosis. In this study, we found that, compared to SP-B-T and WT mice, SP-B-C mice induced more pNF-κB p65 and NLRP3 activation, a higher level of activated Caspase-3, thus causing more apoptosis in the lung of this model.

An accumulating body of evidence showed cytokines such as IL-4 and IL-10, served as anti-inflammatory chemokines whereas TNF-α, IL-1α, IL-1β, IL-6, IFN-γ as pro-inflammatory cytokines (35). In the present study, at the time point of 24 h post-infection, cytokines of TNF-α, IL-1α, IL-1β, IL-6 significantly increased compared to the control group meanwhile the SP-B-C mice demonstrated higher levels than SP-B-T and WT mice. The cytokines IL-4, IL-12, IFN-γ, G-CSF and GM-CSF increased significantly after the infection but no significant difference among the two SP-B genetic variants and WT. By contrast, no increase was observed of cytokines of IL-2, IL-10 and IL-17A between the control and infection groups. The differential response-time to infection may be one of the reasons. For example, IL-17A, as an early pro-inflammatory cytokine, responded to the bacteria infection transiently and returned to the baseline at 24 hrs post-infection (34). The previous study indicated levels of TNF-α, IL-6 rose sharply and reached a peak at 24 hrs after LPS exposure while IL-10 and IFN-γ elevated gradually from 24 hrs and peaked at 96 hrs. However, as to the most-recognized pro-inflammatory cytokines TNF-α, IL-1β and IL-6, their significant differences were observed between infected SP-B-C and SP-B-T mice in this study.

In summary, we have used hTG SP-B-C, SP-B-T, and WT mice to study the regulatory roles of hSP-B genetic variants on the lung injury and the surface activity of pulmonary surfactant in pneumonia-induced sepsis. We found that SP-B genetic variants differentially influenced lung inflammation and tissue injury, as well as surfactant dysfunction in this *P. aeruginosa*-induced sepsis model. The underlying mechanisms of the differential regulation of SP-B T and C variant involved in influencing of bacterial growth and lung cell death, modulating cytokine expression and inflammatory NF-κB signaling activation, as well as regulating surface activity in the lung of infected mice.

Acknowledgments

The authors thank Dr. Jennifer F. Moffat of the Department of Microbiology and Immunology, SUNY Upstate Medical University, Syracuse, NY, for kindly providing the bioluminescent bacterial strain of *P. aeruginosa* Xen5 and *in vivo* imaging system. They also thank all members of Profs. RN Cooney and G. Nieman's laboratories for their kind support to this project.

Conflicts of interest

The authors confirm no competing interests.

Fundings

This work was supported by NIH R01HL136706 and in part by the NSF research award (1722630) (G.W.).

References

1. Whitsett JA and Weaver TE: Hydrophobic surfactant proteins in lung function and disease. *N Engl J Med* 347(26):2141-8, 2002.
2. Yang L, Johansson J, Ridsdale R, Willander H, Fitzen M, Akinbi HT and Weaver TE: Surfactant protein B propeptide contains a saposin-like protein domain with antimicrobial activity at low pH. *J Immunol* 184(2):975-83, 2010.
3. Wang G, Christensen ND, Wigdahl B, Guttentag SH and Floros J: Differences in N-linked glycosylation between human surfactant protein-B variants of the C or T allele at the single-nucleotide polymorphism at position 1580: implications for disease. *The Biochem J* 369(Pt 1):179-84, 2003.
4. Marttila R, Haataja R, Guttentag S and Hallman M: Surfactant protein A and B genetic variants in respiratory distress syndrome in singletons and twins. *Am J Respir Crit Care Med,* 168(10):1216-22, 2003.
5. Taponen S, Huusko JM, Petaja-Repo UE, Paananen R, Guttentag SH, Hallman M and Haataja R: Allele-specific N-glycosylation delays human surfactant protein B secretion in vitro and associates with decreased protein levels in vivo. *Pediatr Res* 74(6):646-51, 2013.
6. Quasney MW, Waterer GW, Dahmer MK, Kron GK, Zhang Q, Kessler LA and Wunderink RG: Association between surfactant protein B + 1580 polymorphism and the risk of respiratory failure in adults with community-acquired pneumonia. *Crit Care Med* 32(5):1115-9, 2004.
7. Dahmer MK, O'Cain P, Patwari PP, Simpson P, Li SH, Halligan N and Quasney MW: The influence of genetic variation in surfactant protein B on severe lung injury in African American children. *Crit Care Med* 39(5):1138-44, 2011.
8. To KKW, Zhou J, Song YQ, Hung IFN, Ip WCT, Cheng ZS, Chan ASF, Kao RYT, Wu AKL, Chau S, et al.: Surfactant protein B gene polymorphism is associated with severe influenza. *Chest* 145(6):1237-1243, 2014.
9. Lin Z, Pearson C, Chinchilli V, Pietschmann SM, Luo J, Pison U and Floros J: Polymorphisms of human SP-A, SP-B, and SP-D genes: association of SP-B Thr131Ile with ARDS. *Clinical genetics* 58(3):181-91, 2000.

10. Simonato M, Baritussio A, Ori C, Vedovelli L, Rossi S, Dalla Massara L, Rizzi S, Carnielli VP and Cogo PE: Disaturated-phosphatidylcholine and surfactant protein-B turnover in human acute lung injury and in control patients. *Respir Res* 12:36, 2011.
11. Schmidt R, Markart P, Ruppert C, Wygrecka M, Kuchenbuch T, Walmrath D, Seeger W and Guenther A: Time-dependent changes in pulmonary surfactant function and composition in acute respiratory distress syndrome due to pneumonia or aspiration. *Respir Res* 8:55, 2007.
12. Bruhn H: A short guided tour through functional and structural features of saposin-like proteins. *Biochem J* 389(Pt 2):249-57, 2005.
13. Brasch F, Johnen G, Winn-Brasch A, Guttentag SH, Schmiedl A, Kapp N, Suzuki Y, Muller KM, Richter J, Hawgood S, et al.: Surfactant protein B in type II pneumocytes and intra-alveolar surfactant forms of human lungs. *Am J Respir Cell Mol Biol* 30(4):449-58, 2004.
14. Guttentag S: Posttranslational regulation of surfactant protein B expression. *Semin Perinatol* 32(5):367-70, 2008.
15. Shultz LD, Brehm MA, Bavari S and Greiner DL: Humanized mice as a preclinical tool for infectious disease and biomedical research. *Ann N Y Acad Sci* 1245:50-4, 2011.
16. Simanainen U, Brogley M, Gao YR, Jimenez M, Harwood DT, Handelsman DJ and Robins DM: Length of the human androgen receptor glutamine tract determines androgen sensitivity in vivo. *Mol Cell Endocrinol* 342(1-2):81-6, 2011.
17. Ge L, Liu X, Chen R, Xu Y, Zuo YY, Cooney RN and Wang G: Differential susceptibility of transgenic mice expressing human surfactant protein B genetic variants to Pseudomonas aeruginosa induced pneumonia. *Biochem Biophys Res Commun* 469(2):171-5, 2016.
18. Xu Y, Ge L, Abdel-Razek O, Jain S, Liu Z, Hong Y, Nieman G, Johnson F, Golub LM, Cooney RN, et al.: Differential Susceptibility of Human Sp-B Genetic Variants on Lung Injury Caused by Bacterial Pneumonia and the Effect of a Chemically Modified Curcumin. *Shock* 45(4):375-84, 2016.
19. McConnell KW, McDunn JE, Clark AT, Dunne WM, Dixon DJ, Turnbull IR, Dipasco PJ, Osberghaus WF, Sherman B, Martin JR, et al.: Streptococcus pneumoniae and Pseudomonas aeruginosa pneumonia induce distinct host responses. *Crit Care Med* 38(1):223-41, 2010.
20. Chroneos ZC, Wert SE, Livingston JL, Hassett DJ and Whitsett JA: Role of cystic fibrosis transmembrane conductance regulator in pulmonary clearance of Pseudomonas aeruginosa in vivo. *J Immunol* 165(7):3941-50, 2000.

21. Liu J, Abdel-Razek O, Liu Z, Hu F, Zhou Q, Cooney RN and Wang G: Role of surfactant proteins a and d in sepsis-induced acute kidney injury. *Shock* 43(1):31-8, 2015.
22. Du J, Abdel-Razek O, Shi Q, Hu F, Ding G, Cooney RN and Wang G: Surfactant protein D attenuates acute lung and kidney injuries in pneumonia-induced sepsis through modulating apoptosis, inflammation and NF-kappaB signaling. *Sci Rep* 8(1):15393, 2018.
23. Yu J, Ni L, Zhang X, Zhang J, Abdel-Razek O and Wang G: Surfactant Protein D Dampens Lung Injury by Suppressing NLRP3 Inflammasome Activation and NF-kappaB Signaling in Acute Pancreatitis. *Shock*, 2018.
24. Milos S, Khazaee R, McCaig LA, Nygard K, Gardiner RB, Zuo YY, Yamashita C and Veldhuizen R: Impact of ventilation-induced lung injury on the structure and function of lamellar bodies. *Am J Physiol Lung Cell Mol Physiol* 313(3):L524-L533, 2017.
25. Valle RP, Wu T and Zuo YY: Biophysical influence of airborne carbon nanomaterials on natural pulmonary surfactant. *ACS Nano* 9(5):5413-21, 2015.
26. Yu K, Yang J and Zuo YY: Automated Droplet Manipulation Using Closed-Loop Axisymmetric Drop Shape Analysis. *Langmuir* 32(19):4820-6, 2016.
27. Hornef MW, Wick MJ, Rhen M and Normark S: Bacterial strategies for overcoming host innate and adaptive immune responses. *Nat Immunol* 3(11):1033-40, 2002.
28. Melton KR, Nesslein LL, Ikegami M, Tichelaar JW, Clark JC, Whitsett JA and Weaver TE: SP-B deficiency causes respiratory failure in adult mice. *Am J Physiol Lung Cell Mol Physiol* 285(3):L543-9, 2003.
29. Hamvas A, Cole FS and Nogee LM: Genetic disorders of surfactant proteins. *Neonatology* 91(4):311-7, 2007.
30. Hamvas A, Heins HB, Guttentag SH, Wegner DJ, Trusgnich MA, Bennet KW, Yang P, Carlson CS, An P and Cole FS: Developmental and genetic regulation of human surfactant protein B in vivo. *Neonatology* 95(2):117-24, 2009.
31. Shultz LD, Ishikawa F and Greiner DL: Humanized mice in translational biomedical research. *Nature reviews. Immunology* 7(2):118-30, 2007.

32. Korimilli A, Gonzales LW and Guttentag SH: Intracellular localization of processing events in human surfactant protein B biosynthesis. *J Biol Chem* 275(12):8672-9, 2000.
33. Whitsett JA: Review: The intersection of surfactant homeostasis and innate host defense of the lung: lessons from newborn infants. *Innate Immun* 16(3):138-42, 2010.
34. Coya JM, Akinbi HT, Saenz A, Yang L, Weaver TE and Casals C: Natural Anti-Infective Pulmonary Proteins: In Vivo Cooperative Action of Surfactant Protein SP-A and the Lung Antimicrobial Peptide SP-BN. *J Immunol* 195(4):1628-36, 2015.
35. Di Paolo NC and Shayakhmetov DM: Interleukin 1alpha and the inflammatory process. *Nat Immunol* 17(8):906-13, 2016.

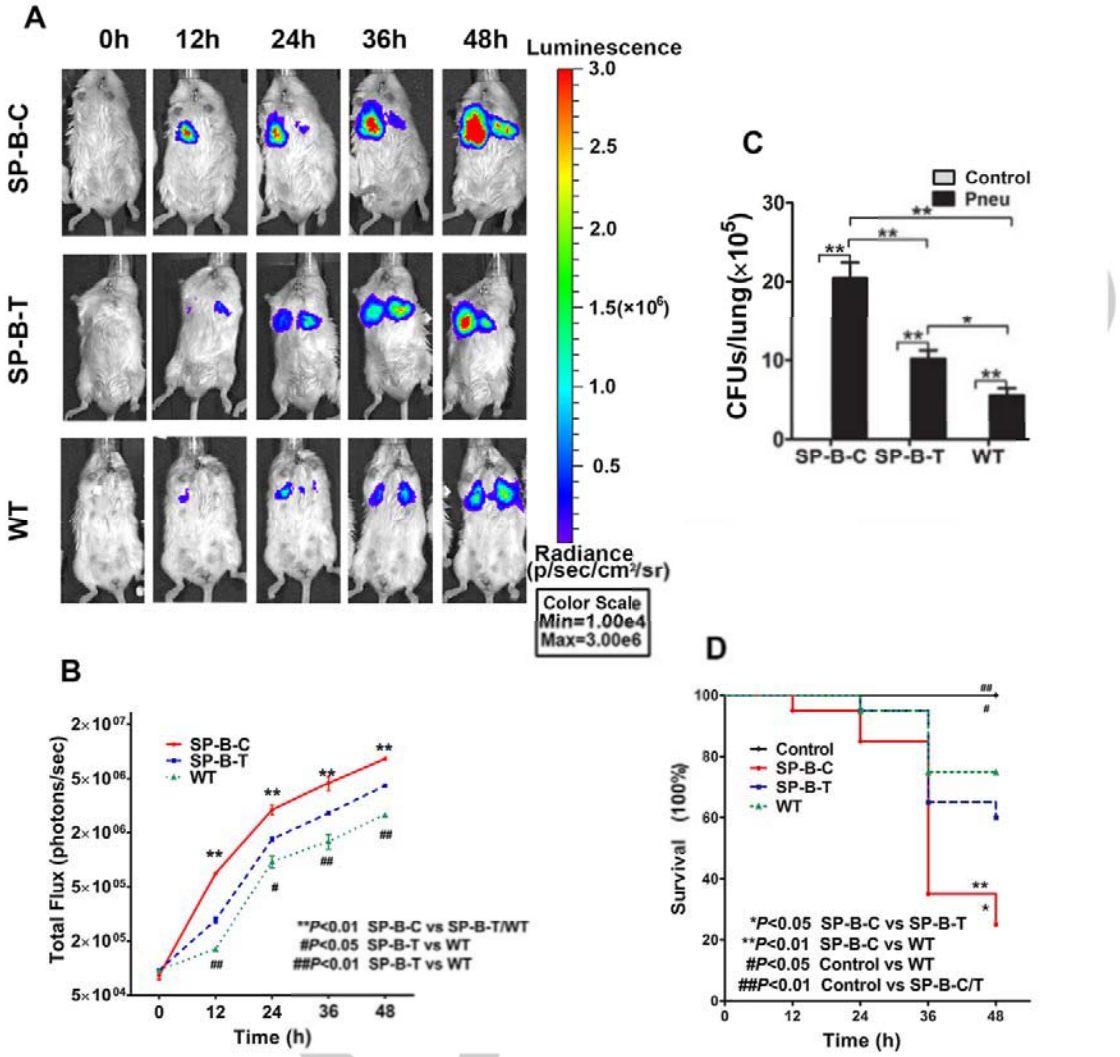

Fig.1. Dynamic changes of bacterial growth *in vivo* and CFUs of BALF in infected SP-B-C, SP-B-T and WT mice.

(A) Representative *in vivo* imaging photos of SP-B-C, SP-B-T and WT mice after intratracheal inoculation of bioluminescent *P. aeruginosa* Xen5. Mice were monitored at 0, 12, 24, 36, and 48 hours after infection for determining bacterial growth *in vivo*. Dynamic bacterial growth in the lung was observed from 12 hrs to 48 hrs after infection in all three types of mice. **(B)** Statistical analysis of bioluminescent levels indicated a significant difference in bacterial burden at several time points among SP-B-C, SP-B-T and WT mice. Graphs are expressed as means ± SEM; n=8 ; ** $P < 0.01$, SP-B-C vs SP-B-T/WT; $^{\#}$ $P < 0.05$, SP-B-T vs WT; $^{\#\#}$ $P < 0.01$, SP-B-T vs WT. **(C)** Bacterial CFUs in the BALF were determined by agar-plate culture. Analysis quantification of bacterial CFUs of BALF showed a significant difference among infected SP-B –C, SP-B-T and WT mice. Graphs are expressed as means ± SEM; n=8 ; *$P < 0.05$, ** P < 0.01. **(D)** Survival curves of infected SP-B-C, SP-B-T and WT mice. The results from the Kaplan-Meier survival analysis showed a higher rate of mortality of infected SP-B-C mice compared to infected SP-T and WT mice. n = 18; * $P < 0.05$, SP-B-C vs SP-B-T; ** $P < 0.01$, SP-B-C vs WT; $^{\#}$ $P < 0.05$, control vs WT; $^{\#\#}$ $P < 0.01$, control vs SP-B-C/T.

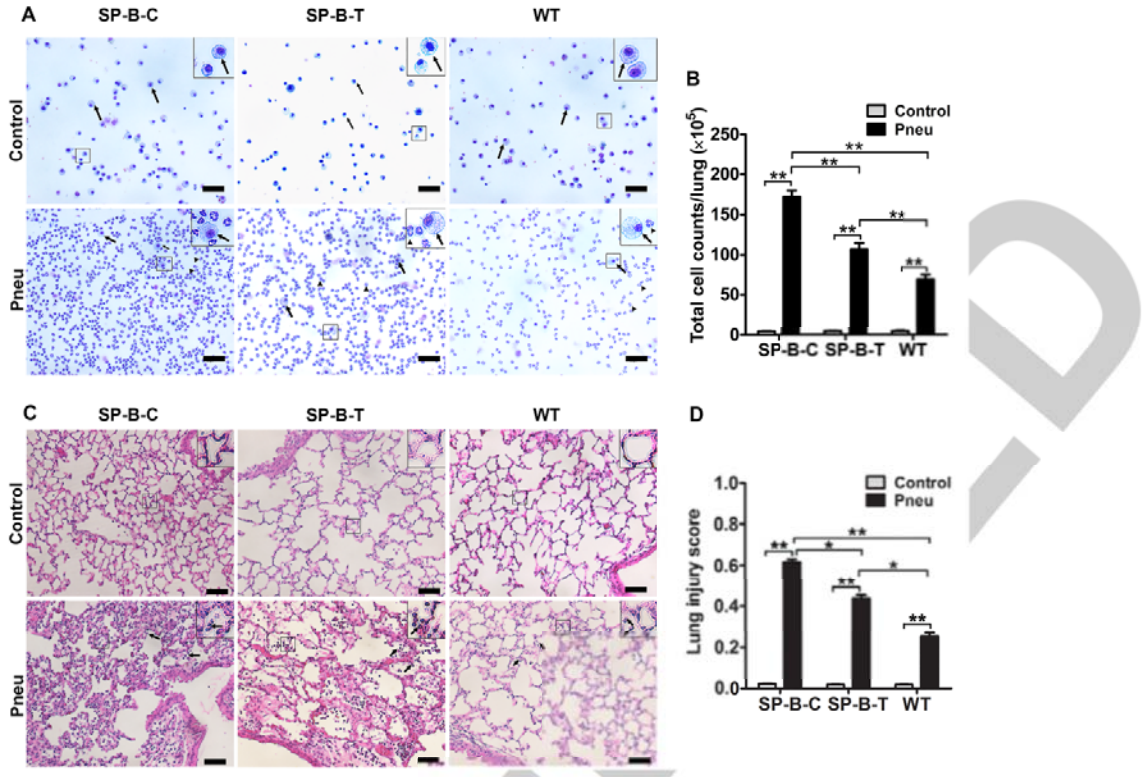

Fig. 2. Inflammatory cells of BALF and lung injury in infected SP-B-C, SP-B-T and WT mice.

(A) A representative of inflammatory cells of BALF isolated from SP-B-C, SP-B-T and WT mice with and without infection. The cells from BALF were mounted on slides by the cytospin centrifugation, then stained with HEMA3 staining kit. The results showed that control mice had macrophages (black arrows), but infected mice (Pneu = Pneumonia) contained more than 90% of neutrophils (black arrowheads). **(B)** The results of statistical analysis of total cell counts indicated increased in the infected mice compared to control, and there are significant differences among infected SP-B-C, SP-B-T and WT mice (SP-B-C > SP-B-T > WT) but not among three types of control mice. Graphs are expressed as means ± SEM; n=8 ; $^{**}P$ <0.01. **(C)** Representative lung histology from control and infected mice. The lung tissues of infected mice (Pneu) showed obvious tissue injury, evidenced by large amounts of inflammation cells (black arrows) filled in alveolar spaces and interstitials, proteinaceous debris accumulation and wider alveolar walls. **(D)** Quantitative analysis of lung injury score indicated that infected SP-B-C mice showed the highest score of lung injury among three types of infected mice. Graphs represented as the mean±SEM; n=8; $^{*}P < 0.05$, $^{**}P < 0.01$. (Magnification 200x, Scale bar = 100 μm)

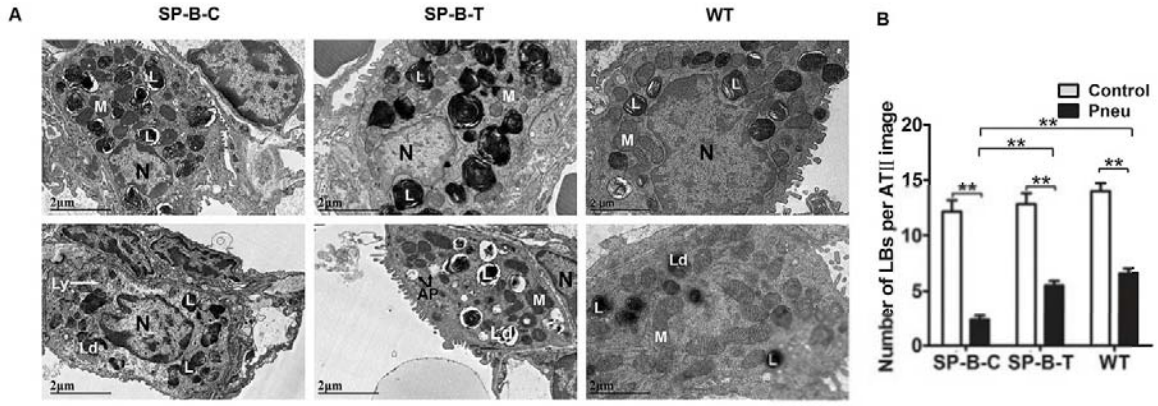

Fig. 3. Ultrastructural analysis of lung tissue by electron microscopy.

(A) The ultrastructures of lung cells were examined by transmission electron microscopy at various magnification from 6,000x to 35,000x. Normal ultrastructural properties of cells were determined in control SP-B-C, SP-B-T, WT mice (Panel control). However, it was observed increased damaged lamellar bodies, injurious mitochondria, and autophagosomes in alveolar type II cells in infected mice (Panel Pneu). N, Nucleus; M, Mitochondria; L, Lamella body; Ld, the damaged lamellar body; AP, autophagosome. (B) There is a decreased number of lamellar bodies in type II cells of infected mice compared to the controls. The number of lamellar bodies of infected SP-C was less than that of infected SP-B-T and WT mice. Graphs represented as the mean±SEM; n=8; $*P < 0.05$, $** P < 0.01$. Scale bar = 2μm.

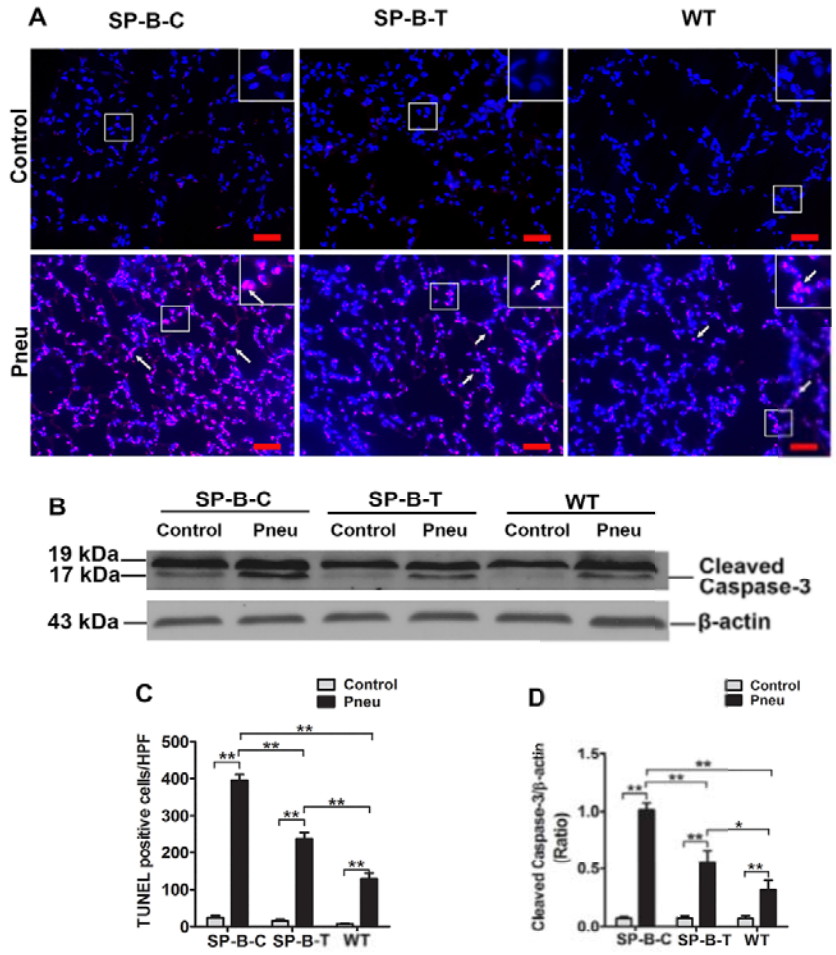

Fig. 4. Apoptosis in the lung of infected SP-B-C, SP-B-T and WT mice.

(A) Representative images of TUNEL assay in the lung section of control and infected mice were shown. The positive apoptotic cells showed pink color (white arrows), blue color pointed out nuclei of all cells (Magnification 200 x, scale bar = 100 μm). Remarkable apoptotic cells were observed in the lung of infected mice but not in the control mice. **(B)** Activated caspase-3 expression (Cleaved caspase-3 band. kDa =17) was examined by Western blotting analysis. The activated caspase-3 band was observed in the lung of infected mice. **(C)** Statistical analysis of apoptotic cells indicated the highest number of TUNEL positive cells in the lung tissue of infected SP-B-C mice among three types of mice. Graphs represented as the mean±SEM; n=8; ** $P < 0.01$. **(D)** Quantitative analysis of activated caspase-3 band (17 kDa) (activated caspase-3/β-actin) revealed that infected SP-B-C mice had the highest activated caspase-3 among three types of infected mice. Graphs represented as the mean±SEM; n=8; *$P < 0.05$, ** $P < 0.01$.

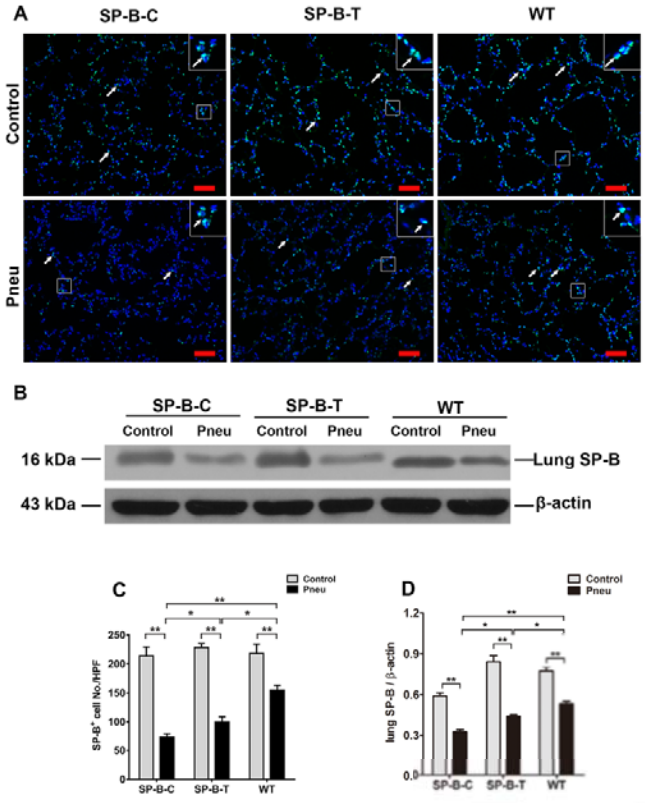

Fig. 5. Decreased levels of SP-B expression in the lungs of infected SP-B-C, SP-B-T and WT mice.

(A) Representative images of SP-B expression by Immunofluorescence analysis in the lungs of control and infected mice. SP-B positive cells showed green color (white arrows), blue color indicated for nuclei of all cells. Decreased SP-B positive cells were observed in the infected lung compared to their control, respectively. (Magnification 200 x, scale bar = 100 μm). **(B)** Protein SP-B expression was examined in the lung tissue by western blotting with an anti-SP-B antibody. The results of the quantitative analysis were shown in panel D. **(C)** Quantitative analysis of SP-B positive cells in the images of IF indicated differential SP-B positive cell number of infected mice (SP-B-C < SP-B-T < WT). Graphs represented as the mean±SEM; n=8; *$P < 0.05$, ** P < 0.01. **(D)** Quantitative analysis of SP-B expression in the lung indicated decreased SP-B level in infected mice compared to control mice. There are different levels among infected mice (SP-B-C < SP-B-T < WT). Graphs represented as the mean±SEM; n=8; *$P < 0.05$, ** $P < 0.01$.

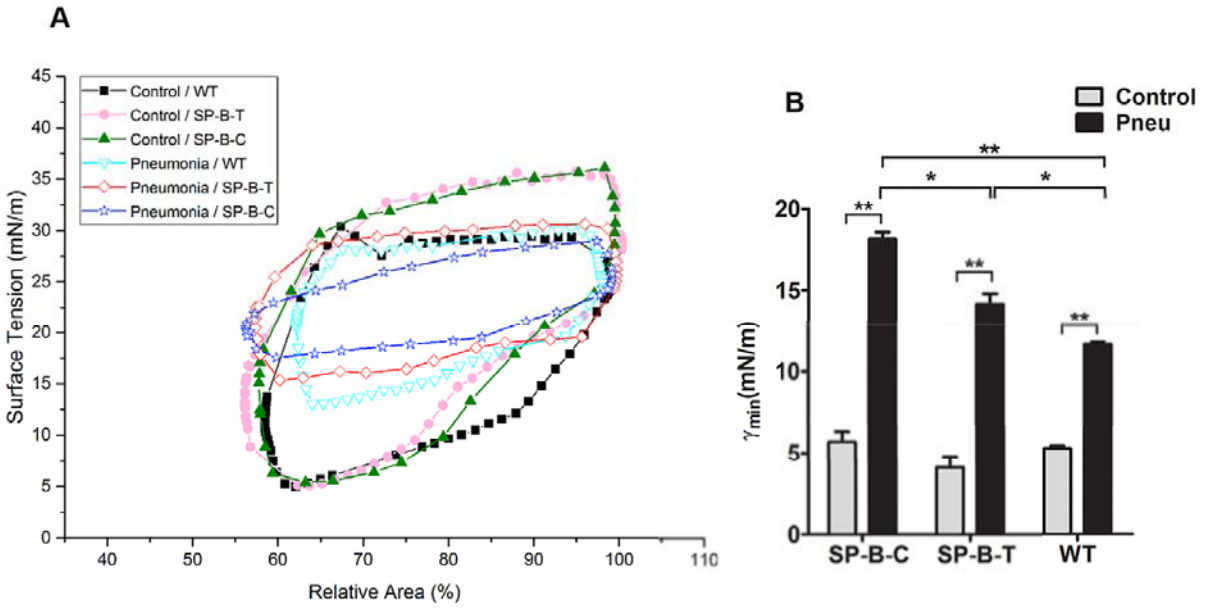

Fig. 6. Surface activity of large aggregates (LAs) from BALF of infected and control SP-B-C, SP-B-T and WT mice.

The surface tension of pulmonary surfactants, i.e., LAs, from BALF was assessed in infected and sham SP-B-C, SP-B-T and WT mice by the CDS method. **(A)** Representative dynamic cycling of infected and control SP-B-C, SP-B-T and WT mice. **(B)** Statistical analysis of the minimum surface tension (γ_{min}) of infected and control mice. Results indicated a significant increase in the γ_{min} of the infected mice compared to the control mice. The γ_{min} of the three infection groups ranks in the order of SP-B-C > SP-B-T > WT. Graphs represented as mean ± SEM; n=9; *$P < 0.05$, ** $P < 0.01$.

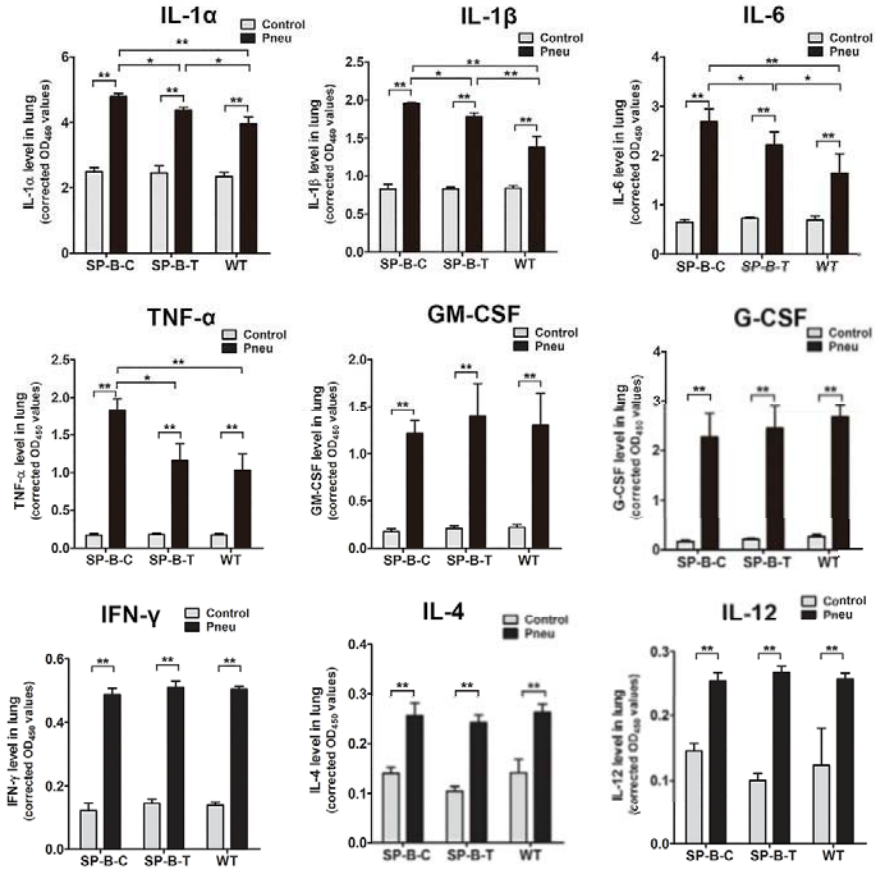

Fig. 7. Analyses of multiple cytokine expression in the lungs of infected SP-B-C, SP-B-T and WT mice.

Multiple cytokine expression was measured in the lung tissues of infected and uninfected mice by A Muti-Analyte ELISArray Kit. Lung tissues were harvested from infected mice at 24hrs post-infection and control mice. The whole lung tissue was homogenized and centrifuged at Eppendorf centrifuge. The supernatant was used for the determination of 12 types of cytokines. The results indicated the increase of nine cytokines (IL-1α, IL-1β, IL-6, TNF-α, GM-CSF, G-CSF, IFN-γ, IL-4, IL-12) and no differences of three cytokines (IL-2, IL-10, IL-17A) in the infected mice compared to control mice. Furthermore, cytokines (IL-1α, IL-1β, IL-6, TNF-α) showed different levels among three types of infected mice (SP-B-C > SP-B-T > WT). Graphs represented as the mean±SEM; n=5; *$P < 0.05$, ** $P < 0.01$.

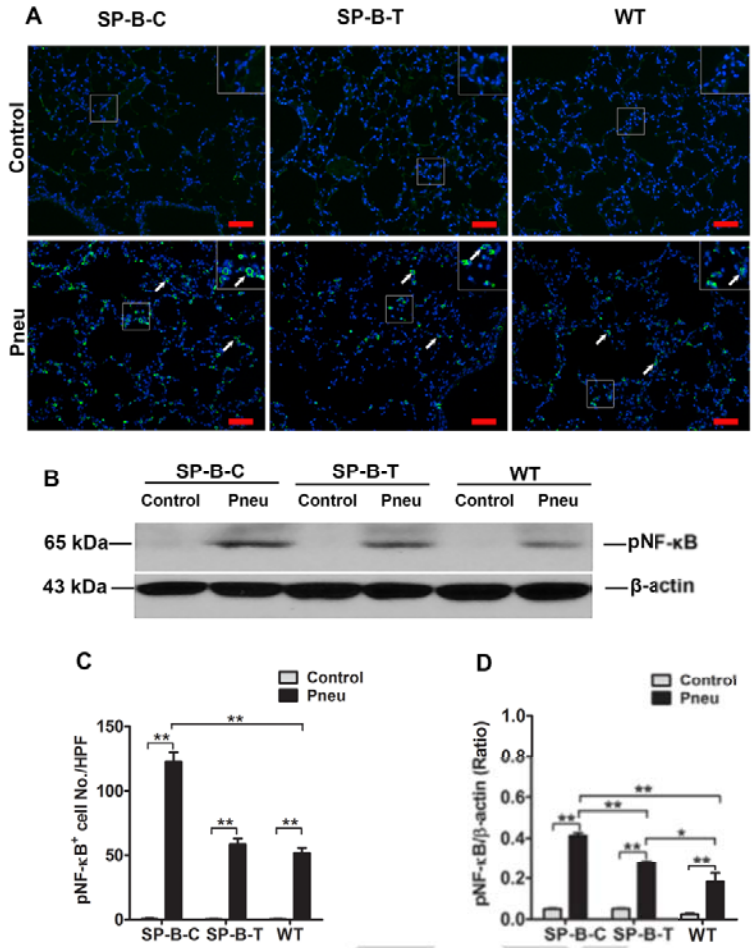

Fig. 8. Increased pNF-κB p65 level in the lungs of infected SP-B-C, SP-B-T and WT mice.

(A) Representative images of NF-κB activation by Immunofluorescence analysis in the lungs of control and infected mice. NF-κB positive cells showed green color (white arrows), blue color indicated for nuclei of all cells. Increased NF-κB positive cells were observed in the infected mice compared to their control, respectively. (Magnification 200 x, scale bar = 100 μm). **(B)** Representative images of pNF-κB expression in the lung of infected SP-B-C, SP-B-T and WT mice and the controls by Western blotting analysis. **(C)** Quantitative analysis of NF-κB positive cells in the images of IF indicated differential SP-B positive cells number of infected mice (SP-B-C >SP-B-T /WT). Graphs represented as the mean±SEM; n=8;** $P < 0.01$. **(D)** Quantitative analysis of pNF-κB level increased in the lungs of infected mice compared to the controls. The data were represented by the ratio of p-NF-κB p65/NF-κB that indicate lung inflammation. Graphs represented as the mean±SEM; n=8; *$P < 0.05$, ** $P < 0.01$.

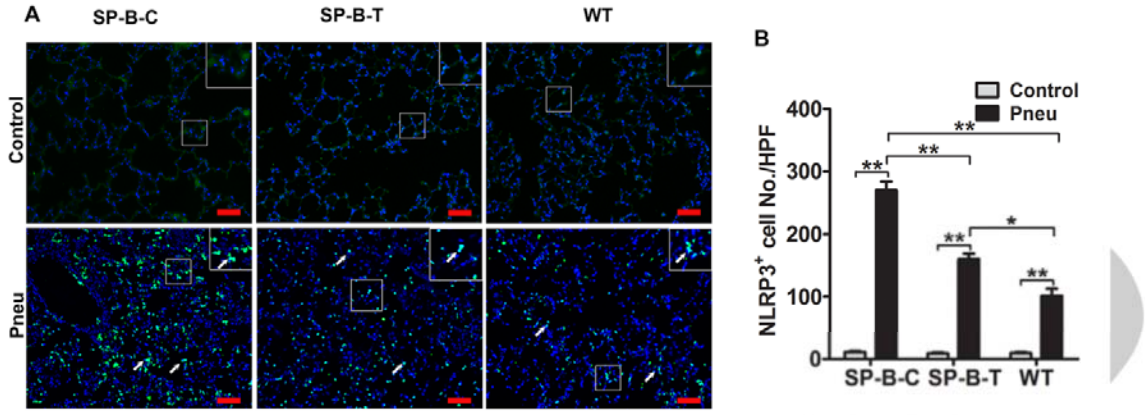

Fig. 9. Increased NLRP3 activation in the lungs of infected SP-B-C compared to infected SP-B-T and WT mice.

(A) Representative images of NLRP3 expression by IF analysis in the lungs of infected mice and controls. NLRP3 positive cells showed green color (white arrows), blue color indicated for nuclei of all cells. Increased NLRP3 positive cells were observed in the infected lung compared to their respective controls. (Magnification 200 x, scale bar = 100 μm). **(B)** Quantitative analysis of NLRP3 positive cells in IF images. The results showed differential NLRP3 activation of infected mice (SP-B-C > SP-B-T > WT). Graphs represented as the mean ± SEM; n=8; *$P < 0.05$, ** $P < 0.01$.